

# Quantum Monte Carlo study of artificial triangular graphene quantum dots

E. Bulut Kul<sup>1</sup>, Gökhan Öztarhan<sup>1</sup>, M. N. Çınar<sup>2</sup>, and A. D. Güçlü<sup>1</sup>  
<sup>1</sup>*Department of Physics, İzmir Institute of Technology, 35430, İzmir, Türkiye*  
<sup>2</sup>*Department of Materials Science and Engineering,  
İzmir Institute of Technology, 35430, İzmir, Türkiye*  
(Dated: June 15, 2025)

We investigate the magnetic phases of triangular graphene quantum dots (TGQDs) with zigzag edges using variational and quantum Monte Carlo methods. These systems serve as quantum simulators for bipartite lattices with broken sublattice symmetry, providing a platform to study the extended Hubbard model's emergent magnetic phenomena, including Lieb's magnetism at half-filling, edge depolarization upon single-electron addition, and Nagaoka ferromagnetism. Our non-perturbative quantum Monte Carlo simulations, performed for lattices of up to 61 sites, reveal that TGQDs transition from metallic to insulating regimes as a function of site radius size, while retaining edge-polarized ground states at half-filling. Notably, edge depolarization occurs upon single-electron doping in both metallic and insulating phases, contrasting with the Nagaoka ferromagnetism observed in hexagonal armchair geometries.

Keywords: artificial graphene, graphene quantum dots, quantum simulators, variational Monte Carlo, diffusion Monte Carlo

Recent advances in the fabrication of artificial superlattices provide reliable quantum simulators, allowing to replicate known physical phenomena in more accessible lengths and desired energy scales, as well as to predict new physics[1–13]. Among these superlattices, artificial graphene nanostructures, realized through cold atoms[14–16] and semiconductor heterojunctions[17–19], have proven to be good platforms for investigating the physics of massless Dirac fermions. Recent observation of graphene-like behaviour in nanopatterned AlGaAs/GaAs quantum wells are advantageous for realizing specific physical properties, particularly due to the ease of fabrication and the precise tuning of parameters, such as the Hubbard parameter  $U/t$  [18, 19]. In light of these advancements, subsequent theoretical studies have emerged focusing on specific sizes and shapes of artificial graphene quantum dots, such as triangular-shaped graphene quantum dots with zigzag edges [20–26].

Triangular zigzag graphene quantum dots (TGQDs) have garnered significant attention due to their unique electronic and magnetic properties[27–30]. Unlike other GQDs, the distinct shape and edge structure of triangular zigzag-edged GQDs lead to localized edge states that exhibit magnetic moments in agreement with Lieb's theorem, making them especially promising for spintronic applications[31–33]. Furthermore, the triangular zigzag edges allow tunable optical and electronic properties through size control, making them versatile for applications in quantum computing, photovoltaics, and catalysis[34–37]. The importance of GQDs lies not only in their potential for advanced technological applications but also in their ability to shed light on fundamental quantum mechanical behaviors in low-dimensional systems [38–40].

A particularly interesting property of real TGQDs is the edge depolarization effect, which is predicted by configuration interaction calculations performed in the subspace of degenerate edge orbitals. When an extra elec-

tron is added to the edge polarized charge neutral system, edge magnetization is lost[29, 41], allowing optical control of magnetic and transport properties[34]. This depolarization property was recently investigated in the context of semiconductor-based artificial TGQDs again using a configuration interaction approach within the degenerate edge band[20]. It was found that while a ground state spin depolarization does not occur as an electron is added, the relatively large gap separating the spin-polarized ground state from other states drops dramatically making the edge polarization unstable.

To the best of our knowledge, no other methodology than the configuration interaction was used to confirm the collapse of the edge magnetism in real or artificial TGQDs, presumably due to the fact that the depolarization is a strong correlation effect which does not manifest in mean-field approximation-based calculations. On the other hand, in semiconductor-based artificial TGQDs, the Hubbard parameter  $U/t$  can be of the order of 100[21], i.e. two orders of magnitude larger than in real TGQDs. As a result, the energy gap protecting the edge states from the rest can become significantly smaller than electron-electron interaction scale, casting doubt on the accuracy of perturbative approaches. Moreover, recent work has shown that the addition of a single electron can induce Nagaoka ferromagnetism in hexagonal armchair-type artificial graphene nanostructures[42]. Whether this mechanism competes with edge depolarization remains an open question. Furthermore, the applicability of Lieb's theorem for the Hubbard  $U/t$  model to semiconductor artificial structures is not immediately clear, particularly in cases where long-range interactions and the next-nearest-neighbor tight-binding(TB) hopping term  $t'$  may play a significant role [21]. In this work, we employ non-perturbative continuum variational Monte Carlo (VMC) and diffusion Monte Carlo (DMC) methods to systematically investigate the applicability of Lieb's theorem at

half-filling, the emergence of edge depolarization effects, and the stability of Nagaoka ferromagnetism in charged TGQDs of varying sizes ( $N_s = 33, 46, 61$ ).

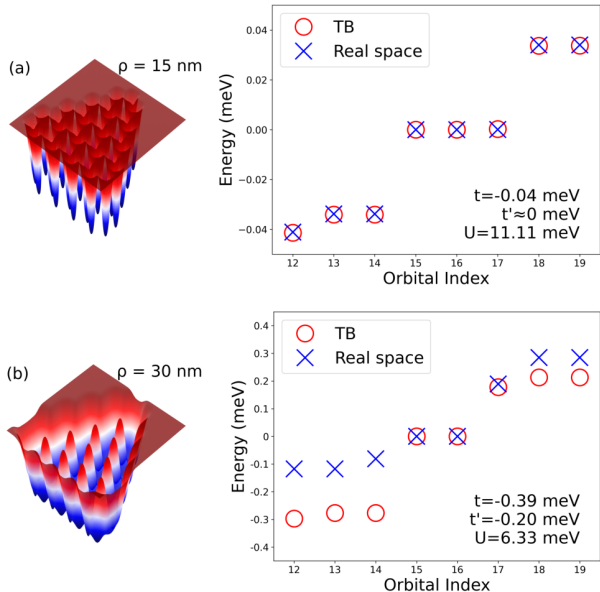


FIG. 1. Potential profiles (left panels) and single particle spectra (right panels) for 33 site TGQD constructed using gaussian-like potentials with radius (a)  $\rho = 15$  nm and (b)  $\rho = 30$  nm. Energy spectra are obtained using real space finite differences method and compared to TB solutions with fitted parameters.

The system of  $N$  interacting electrons in a honeycomb array of  $N_s$  confining potentials is described by the many-body Hamiltonian

$$H = -\frac{1}{2} \sum_i^N \nabla_i^2 + \sum_i^N V(\mathbf{r}_i) + \sum_i^N k|\mathbf{r}_i|^2 + \sum_{i<j}^N \frac{1}{r_{ij}} \quad (1)$$

in effective atomic units (electronic charge  $e$ , dielectric constant  $\epsilon$ , effective mass  $m^*$ , and  $\hbar$  are set to 1), where  $k$  is the spring constant of quadratic gate potential located at the center of the system which controls the finite size effects[21].  $V(\mathbf{r}_i)$  is the total potential energy of the confining potentials, and typical material properties for GaAs, effective electron mass  $m^* = 0.067m_0$  and dielectric constant  $\epsilon = 12.4$ , are used. Corresponding effective Bohr radius is  $a_0^* = 9.794$  nm, and the effective Hartree energy is 11.857 meV. The honeycomb array of potential wells is modelled using gaussian-like functions [43],

$$V(\mathbf{r}) = V_0 \sum_k^{N_s} \exp[-(|\mathbf{r} - \mathbf{R}_k|^2/\rho^2)^s] \quad (2)$$

where  $V_0$  is the potential depth,  $\rho$  is the radius and  $s$  controls the sharpness of the potential wells located at  $\mathbf{R}_k$ . In our numerical calculations, dot-to-dot (nearest neighbor) distance and gaussian sharpness value are fixed to

$a = 50$  nm and  $s = 1.4$ .  $V_0$  values vary depending on the dot radius and system size, seeking the charge neutrality condition as in our previous work [21]. A 3D visualization of 33 artificial TGQD sites constructed using Gaussian-like potentials shown in Fig. 1 for  $\rho = 15$  nm and  $\rho = 30$  nm.

In our calculations, trial wave functions were first obtained using TB and mean-field Hubbard(MFH) orbitals, to build a Slater-Jastrow trial wave functions. While TB-based trial wave functions are well suited to describe metallic phases, adjustable  $U/t$  ratio of MFH method allows for the generation of both liquid-like ( $U/t = 2$ ) and localized ( $U/t = 20$ ) trial wave functions. Further, the trial wave functions were optimized using the VMC method and then fed into the fixed-node diffusion Monte Carlo (DMC) calculations. This allowed us to obtain more accurate upper-bound to the many-electron ground state of artificial TGQDs for neutral and gated systems. Variational and fixed-node energies of those three types of orbitals are expected to hint us at a possible transition from metallic state to an AF order as a function of  $\rho$ . In this work, all quantities that do not commute with the Hamiltonian were calculated using an extrapolated estimator,  $\langle \hat{O} \rangle = 2\langle \hat{O} \rangle_{DMC} - \langle \hat{O} \rangle_{VMC}$  [44].

Before investigating the many-body effects, we study single particle properties computed using finite differences (FD) method using a  $1001 \times 1001$  grid, for a 33 site TGQD shown in Fig. 1. For  $\rho = 15$  nm, the degenerate orbitals 15, 16 and 17 constitute the edge states as predicted by TB method. A fit of FD to TB spectrum reveals that the hopping parameter is given by  $t = -0.04$  meV and the second nearest-neighbor hopping  $t'$  is negligibly small. An estimation of the Hubbard parameter for a single site using  $U = 2\pi \int r n(r) V_e(r) dr$  (and verified through our QMC results) gives 11.11 meV, approximately 200 times larger than  $t$ . On the other hand, for  $\rho = 30$  nm, the value of second nearest neighbor  $t'$  approaches  $t$ : TB approach does not provide a good approximation and a good fit between FD and TB can not be obtained. More importantly, the edge states with orbital indices 15, 16 and 17 are not protected by a gap anymore and their degeneracy is broken. We also note that the confinement potential shape obtained using large  $\rho$  mimics honeycomb lattice obtained using a triangular lattice of antidots[18], as can be seen on the left panel of Fig. 1b. In the following, we will investigate many-body ground states for various values of  $\rho$  between 15 – 35 nm, for half-filled and charged systems.

In Fig. 2a, we investigate the ground state total spin ( $S$ ) for half-filled (charge neutral) system with  $N_s = 33$  sites as a function  $\rho$ . The three degenerate states discussed above host 3 electrons which can have total spin  $S = 1/2$  or  $3/2$ . According to Lieb's theorem which applies to Hubbard model with no long-range interactions, total spin must be half of the difference between the number of atoms in sublattices  $A$  and  $B$ , i.e.  $S = (N_A - N_B)/2 = 3/2$ . Our QMC trial wave functions that were built in the subspaces of  $z$ -projection of spin using

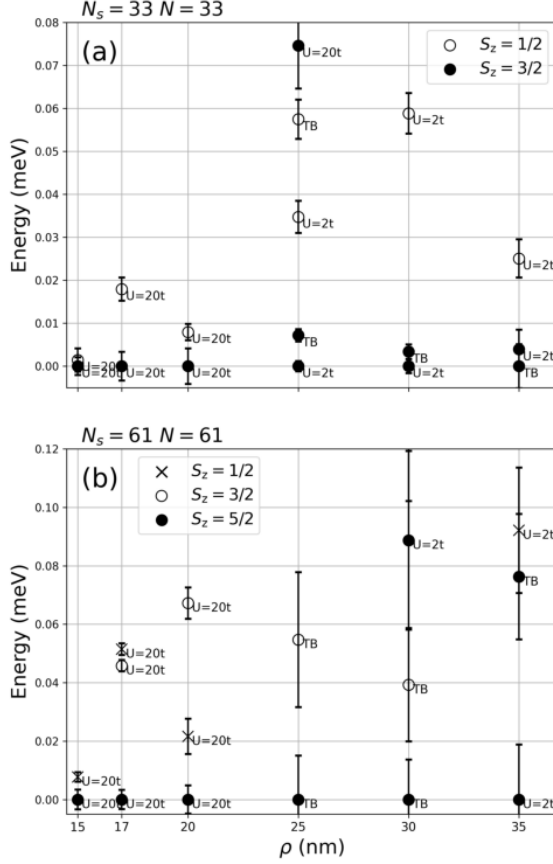


FIG. 2. Diffusion Monte Carlo energies for charge neutral TGQDs as a function of site radius  $\rho$  for (a)  $N_s = 33$  sites and (b)  $N_s = 61$  sites, for all possible spin excitations within edge states, obtained using various trial wave functions.

Hubbard and TB orbitals systematically leads to ground states with  $S_z = 3/2$  in agreement with Lieb's theorem. Moreover, for lower values of  $\rho$ , the  $U = 20t$  trial wave function gives a better fixed-node energy, whereas for larger  $\rho$  values,  $U = 2t$  or TB based trial wave functions are better. Similar results were obtained for a  $N_s = 61$  sites TGQD, shown in Fig. 1b. Since the system now exhibits 5 degenerate edge states, we scanned the subspaces  $S_z = 1/2, 3/2$ , and  $5/2$  using Hubbard and TB trial wave functions, and found that edge states are polarized, giving  $S_z = 5/2$  ground state for all  $\rho$  values.

Next, we focus on whether the spin depolarization effect predicted for real TGQDs structures is also valid for artificial TGQDs, which manifests itself as minimum total spin ( $S$ ) when an extra electron is added to the neutral system [45]. TGQD with 33 sites and 34 electrons have 2 competing spin configurations,  $S_z = 1$  and  $S_z = 0$ . Our numerical results show that, while the energy differences are considerably small, depolarization occurs  $\rho$  between 15 and 35 nm, for as can be seen in Fig. 3a. For the larger structure with 61 sites and 62 electrons (Fig.

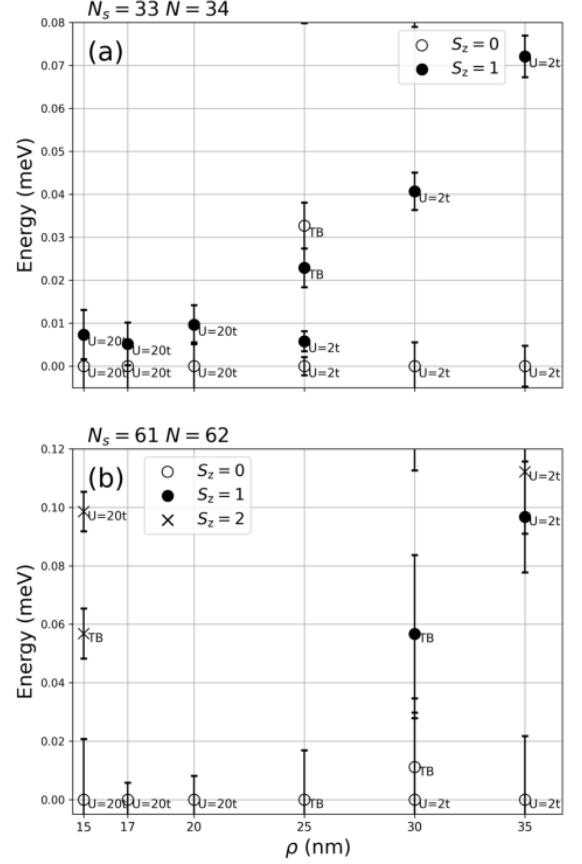


FIG. 3. Diffusion Monte Carlo energies for TGQDs with an additional electron as a function of site radius  $\rho$  for (a)  $N_s = 33$  sites and (b)  $N_s = 61$  sites, for all possible spin excitations within edge states, obtained using various trial wave functions.

3b), the depolarization effect is even stronger, i.e. with a larger gap separating  $S_z = 1$  and  $S_z = 0$  configurations.

In Fig. 4, we investigate the internal spin structure of charge neutral and charged systems with  $N_s = 33, 46, 61$  sites. In our previous work[21], we showed that charge neutral hexagonal armchair and triangular zigzag artificial graphene dots go through a metallic to AFM phase transition around  $\rho = 20$  nm as the radius is decreased. In order to investigate whether a similar transition occurs for gated systems, we consider a real-space spin-spin correlation function averaged over all nearest neighbors  $(i, j)$ , defined as  $g_p = \langle m_i m_j \rangle / \langle n_i n_j \rangle$ , where  $m_i$  and  $n_i$  are the average magnetization and electron density at the site  $i$  within a radius  $r = a/2$ . To reveal the internal spin structure,  $m_i$  and  $n_i$  are calculated from pair densities  $p_{\sigma\sigma_0}(r, r_0)$ , the probability of finding an electron with spin  $\sigma$  at location  $r$  when an electron with spin  $\sigma_0$  is fixed at location  $r_0$ . The output values of the spin-spin correlation function remain in the  $[-1, 1]$  range, with  $g_p = -1$  corresponding to AFM and  $g_p = 0$  corresponding to the metallic configuration. Interestingly, Fig. 4a shows that

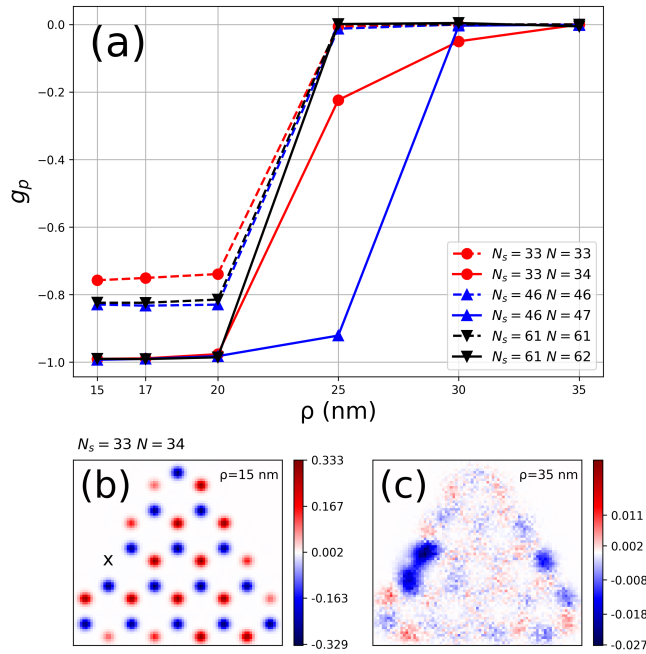


FIG. 4. (a) Extrapolated spin-spin correlation functions  $g_p$  obtained via pair densities for neutral and gated TGQDs with  $N_s = 33, 46$ , and  $61$  sites. (b,c) Extrapolated pair-density results for  $N_s = 33$  and  $N = 34$ , corresponding to the ground state at  $\rho = 15$  nm and  $35$  nm. Fixed reference electron position is marked by  $x$ .

a metallic to AFM transition also takes place when the system is charged with an electron (solid lines). At lower values of  $\rho$ ,  $g_p$  is close to  $-1$ . Although such a perfect AFM behavior is not possible in principle when the system hosts an extra electron,  $g_p$  reaches approximately  $-0.8$  showing relatively strong AFM behavior. This is visualized in Figs. 4a and 4b, showing the pair spin density  $p_{\uparrow\uparrow}(r, r_0) - p_{\downarrow\uparrow}(r, r_0)$  where the reference spin up electron fixed on top of a site is shown with a cross. For  $\rho = 15$  nm, AFM configuration is clearly visible, whereas for  $\rho = 35$  nm only short range spin-spin correlation is observed near the fixed electron, indicating metallic behavior.

Another possible magnetic phase transition induced by the addition of a single charge in graphene quantum dots is Nagaoka ferromagnetism[42, 46]. Initially predicted in the infinite on-site repulsion limit ( $U \rightarrow \infty$ ) of the strongly correlated Hubbard model, Nagaoka ferromagnetism is expected to occur in the presence of a hole (and electron if electron-hole symmetry is present) in a half-filled lattice. It was recently shown in Ref.42 that realistic artificial graphene nanostructures with hexagonal armchair geometry exhibit Nagaoka ferromagnetic phase stabilized by Coulomb scattering mechanisms in addition to the Hubbard  $U$ -term. This phenomenon was overlooked in previous literature examining the single-electron induced edge depolarization in TGQDs. In order to investigate the possibility that Nagaoka ferromag-

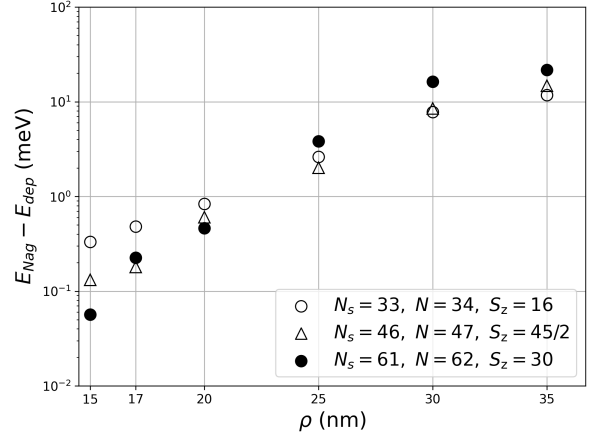


FIG. 5. Diffusion Monte Carlo energy difference between Nagaoka ferromagnetic state and edge-depolarized state,  $E_{Nag} - E_{dep}$  for  $N_s = 33, 46$  and  $61$  site TGQDs, showing that Nagaoka ferromagnetism does not occur as ground state.

netism occurs in artificial TGQDs, in Fig. 5 we show the energy difference between the Nagaoka and edge-depolarized phases,  $E_{Nag} - E_{dep}$  for  $N_s = 33, 46$  and  $61$  site structures. Across the investigated parameter range, we observe no signatures of Nagaoka ferromagnetism. This absence can be attributed to the presence of zigzag edges, which not only break the electron-hole symmetry and also violate the connectivity condition[46] required for the Nagaoka phase, in contrast to hexagonal armchair-edged systems.

In conclusion, we investigated magnetic phases in charge neutral and gated semiconductor artificial TGQDs up to  $61$  sites, using continuum QMC methods, as a function of site the radius  $\rho$ . For half-filled lattice, the system remains edge-polarized being consistent with Lieb's theorem, while going from metallic phase to AFM insulator phase as the site radius is decreased. If a single electron is added to the system, spin depolarization of the edge states occurs in both the metallic and the insulator regimes, validating with previous predictions based on exact diagonalization results. We have also investigated whether the system becomes fully polarized due to Nagaoka ferromagnetism. In contrast with previous recent work on hexagonal armchair artificial graphene flakes, we have not observed emergence of ferromagnetism as a ground state when an electron is added, presumably due to presence of zigzag edges breaking the electron-hole symmetry and violating the connectivity condition. These observations highlight the dependence of magnetic correlations on system geometry and finite-size effects, as revealed through a Hamiltonian model that explicitly include long-range and exchange interactions, thereby offering insight into the potential applicability of artificial TGQDs in quantum simulation and spintronic applications.

## ACKNOWLEDGMENTS

We thank Pawel Potasz for valuable conversations. This work was supported by The Scientific and Tech-

nological Research Council of Turkey (TUBITAK) under the 1001 Grant Project Number 119F119. The numerical calculations reported in this study were partially performed at TUBITAK ULAKBIM, High Performance and Grid Computing site (TRUBA resources).

- 
- [1] I. Bloch, *Nat. Phys.* **1**, 23 (2005).
- [2] A. Mazurenko, C. S. Chiu, G. Ji, M. F. Parsons, M. Kanász-Nagy, R. Schmidt, F. Grusdt, E. Demler, D. Greif, and M. Greiner, *Nature* **545**, 462 (2017).
- [3] H. Weimer, M. Müller, I. Lesanovsky, P. Zoller, and H. P. Büchler, *Nat. Phys.* **6**, 382 (2010).
- [4] R. Islam, E. E. Edwards, K. Kim, S. Korenblit, C. Noh, H. Carmichael, G.-D. Lin, L.-M. Duan, C.-C. Joseph Wang, J. K. Freericks, *et al.*, *Nat. Commun.* **2**, 377 (2011).
- [5] C. Hempel, C. Maier, J. Romero, J. McClean, T. Monz, H. Shen, P. Jurcevic, B. P. Lanyon, P. Love, R. Babbush, *et al.*, *Phys. Rev. X* **8**, 031022 (2018).
- [6] I. Buluta and F. Nori, *Science* **326**, 108 (2009).
- [7] S. Kuhr, *Natl. Sci. Rev.* **3**, 170 (2016).
- [8] J. Salfi, J. A. Mol, R. Rahman, G. Klimeck, M. Y. Simmons, L. C. L. Hollenberg, and S. Rogge, *Nat. Commun.* **7**, 11342 (2016).
- [9] A. Aspuru-Guzik and P. Walther, *Nat. Phys.* **8**, 285 (2012).
- [10] J. Cai, A. Retzker, F. Jelezko, and M. B. Plenio, *Nat. Phys.* **9**, 168 (2013).
- [11] H. Bernien, S. Schwartz, A. Keesling, H. Levine, A. Omran, H. Pichler, S. Choi, A. S. Zibrov, M. Endres, M. Greiner, *et al.*, *Nature* **551**, 579 (2017).
- [12] T. Li, S. Jiang, L. Li, Y. Zhang, K. Kang, J. Zhu, K. Watanabe, T. Taniguchi, D. Chowdhury, L. Fu, *et al.*, *Nature* **597**, 350 (2021).
- [13] S.-A. Guo, Y.-K. Wu, J. Ye, L. Zhang, W.-Q. Lian, R. Yao, Y. Wang, R.-Y. Yan, Y.-J. Yi, Y.-L. Xu, B.-W. Li, Y.-H. Hou, Y.-Z. Xu, W.-X. Guo, C. Zhang, B.-X. Qi, Z.-C. Zhou, L. He, and L.-M. Duan, *Nature* **630**, 613 (2024).
- [14] P. Soltan-Panahi, J. Struck, P. Hauke, A. Bick, W. Plenkers, G. Meineke, C. Becker, P. Windpassinger, M. Lewenstein, and K. Sengstock, *Nature Physics* **7**, 434 (2011).
- [15] L. Tarruell, D. Greif, T. Uehlinger, G. Jotzu, and T. Esslinger, *Nature* **483**, 302 (2012).
- [16] T. Uehlinger, G. Jotzu, M. Messer, D. Greif, W. Hofstetter, U. Bissbort, and T. Esslinger, *Phys. Rev. Lett.* **111**, 185307 (2013).
- [17] G. De Simoni, A. Singha, M. Gibertini, B. Karmakar, M. Polini, V. Piazza, L. N. Pfeiffer, K. W. West, F. Beltram, and V. Pellegrini, *Applied Physics Letters* **97**, 132113 (2010), <https://pubs.aip.org/aip/apl/article-pdf/doi/10.1063/1.3493189/13663475/132113.1.online.pdf>.
- [18] L. Du, S. Wang, D. Scarabelli, L. N. Pfeiffer, K. W. West, S. Fallahi, G. C. Gardner, M. J. Manfra, V. Pellegrini, S. J. Wind, *et al.*, *Nat. Commun.* **9**, 3299 (2018).
- [19] S. Wang, D. Scarabelli, L. Du, Y. Y. Kuznetsova, L. N. Pfeiffer, K. W. West, G. C. Gardner, M. J. Manfra, V. Pellegrini, S. J. Wind, *et al.*, *Nat. Nanotechnol.* **13**, 29 (2018).
- [20] Y. Saleem, A. Dusko, M. Cygorek, M. Korkusinski, and P. Hawrylak, *Phys. Rev. B* **105**, 205105 (2022).
- [21] G. Öztarhan, E. B. Kul, E. Okcu, and A. D. Güçlü, *Phys. Rev. B* **108**, L161114 (2023).
- [22] R. Ortiz, G. Catarina, and J. Fernández-Rossier, *2D Materials* **10**, 015015 (2022).
- [23] H. Abdelsalam, O. H. Abd-Elkader, M. A. Sakr, N. H. Tebeb, V. A. Saroka, and Q. Zhang, *Physica E: Low-dimensional Systems and Nanostructures* **164**, 116059 (2024).
- [24] L. Madail, R. G. Dias, and J. Fernández-Rossier, *Phys. Rev. Res.* **6**, 043262 (2024).
- [25] Y. Saleem, T. Steenbock, E. R. J. Alhadi, W. Pasek, G. Bester, and P. Potasz, *Nano Letters* **24**, 7417 (2024).
- [26] A. Garcia-Ruiz and M.-H. Liu, *Nano Letters* 10.1021/acs.nanolett.4c04556 (2024).
- [27] P. Potasz, A. D. Güçlü, O. Voznyy, J. A. Folk, and P. Hawrylak, *Phys. Rev. B* **83**, 174441 (2011).
- [28] A. D. Güçlü, P. Potasz, M. Korkusinski, and P. Hawrylak, *Graphene Quantum Dots* (Springer, Berlin, Heidelberg, 2014).
- [29] P. Potasz, A. D. Güçlü, A. Wójs, and P. Hawrylak, *Phys. Rev. B* **85**, 075431 (2012).
- [30] R. Han, J. Chen, M. Zhang, J. Gao, Y. Xiong, Y. Pan, and T. Ma, *Phys. Rev. B* **109**, 075117 (2024).
- [31] H. Şahin, R. T. Senger, and S. Ciraci, *Journal of Applied Physics* **108**, 074301 (2010), <https://pubs.aip.org/aip/jap/article-pdf/doi/10.1063/1.3489919/13195697/074301.1.online.pdf>.
- [32] Y. Sun, Y. Zheng, H. Pan, J. Chen, W. Zhang, L. Fu, K. Zhang, N. Tang, and Y. Du, *npj Quantum Materials* **2**, 5 (2017).
- [33] S. S. Gregersen, S. R. Power, and A.-P. Jauho, *Phys. Rev. B* **95**, 121406 (2017).
- [34] A. D. Güçlü and P. Hawrylak, *Phys. Rev. B* **87**, 035425 (2013).
- [35] Y. Li, H. Shu, S. Wang, and J. Wang, *The Journal of Physical Chemistry C* **119**, 4983 (2015).
- [36] X. Wang, G. Sun, N. Li, and P. Chen, *Chem. Soc. Rev.* **45**, 2239 (2016).
- [37] Y. El Haddad, H. Ouarrad, and L. B. Drissi, *RSC Adv.* **14**, 12639 (2024).
- [38] C. Gutiérrez, D. Walkup, F. Ghahari, C. Lewandowski, J. F. Rodriguez-Nieva, K. Watanabe, T. Taniguchi, L. S. Levitov, N. B. Zhitenev, and J. A. Stroscio, *Science* **361**, 789 (2018), <https://www.science.org/doi/pdf/10.1126/science.aar2014>.
- [39] S.-Y. Li and L. He, *Frontiers of Physics* **17**, 33201 (2021).
- [40] K. S. Hong, O. Chen, and Y. Bai, *Nano Research* **17**, 10490 (2024).
- [41] A. D. Güçlü, P. Potasz, O. Voznyy, M. Korkusinski, and P. Hawrylak, *Phys. Rev. Lett.* **103**, 246805 (2009).
- [42] G. Öztarhan, P. Potasz, and A. D. Güçlü, *Nagaoka ferromagnetism in semiconductor artificial graphene* (2025),

- arXiv:2504.01492 [cond-mat.mes-hall].
- [43] I. Kylänpää, F. Berardi, E. Räsänen, P. García-González, C. A. Rozzi, and A. Rubio, *New J. Phys.* **18**, 083014 (2016).
- [44] W. M. C. Foulkes, L. Mitas, R. J. Needs, and G. Rajagopal, *Rev. Mod. Phys.* **73**, 33 (2001).
- [45] A. D. Güçlü, P. Potasz, O. Voznyy, M. Korkusinski, and P. Hawrylak, *Phys. Rev. Lett.* **103**, 246805 (2009).
- [46] Y. Nagaoka, *Phys. Rev.* **147**, 392 (1966).